JOURNAL OF AIRCRAFT
Vol. 42, No. 6, November–December 2005

Effect of Tip Vortex on Wing Aerodynamics of Micro Air Vehicles

Dragos Viieru,* Roberto Albertani,* Wei Shyy,† and Peter G. Ifju‡
University of Florida, Gainesville, Florida 32611

Tip vortex induces downwash movement, which reduces the effective angle of attack of a wing. For a low-aspect-ratio, low-Reynolds-number wing, such as that employed by the micro air vehicle (MAV), the induced drag by the tip vortex substantially affects its aerodynamic performance. In this paper we use the endplate concept to help probe the tip-vortex effects on the MAV aerodynamic characteristics. The investigation is facilitated by solving the Navier–Stokes equations around a rigid wing with a root-chord Reynolds number of 9×10^4. It is confirmed that with modest angles of attack the endplate can improve the lift-to-drag ratio by reducing the drag. However, as the angle of attack becomes substantial, the wing tip vortex is stronger and the endplate loses its effectiveness. Detailed fluid flow structures are presented to offer insight into the physics responsible for the observed phenomena.

Nomenclature

AR	=	wing aspect ratio
C_D	=	drag coefficient
C_L	=	lift coefficient
C_p	=	pressure coefficient
c	=	wing-root-chord length
D	=	drag force
L	=	lift force
Re	=	Reynolds number
u	=	X component (horizontal) of the velocity
v	=	Y component (vertical) of the velocity
w	=	Z component (lateral) of the velocity

Introduction

MICRO air vehicles (MAVs) with a maximal dimension of 15 cm or smaller, and a flight speed of about 10 m/s, are of interest for both military and civilian applications.[1] As MAVs reduce their dimensions, structural strength and the stall angle become more favorable. However, the small dimension and low flight speed result in a low-Reynolds-number flight regime in the range of 10^4–10^5. Based on biological inspiration and theoretical investigation,[1] as well as our experience gained from vehicle development efforts,[2] we have identified suitable parameters for the MAV wing, including airfoil thickness and camber characteristics. Furthermore, we find that membrane wings can help the aerodynamic performance by delaying stall and adapting to wind gust.

This study and a previous effort[3] focus on a 15 cm MAV designed by Ifju and coworkers[2] shown in Fig. 1. The vehicle, powered by an electric motor, flies at speeds between 20 and 40 km/h while carrying a video camera and a transmitter. A unique aspect of this MAV is its low-aspect-ratio flexible membrane wing. The cambered wing structure is constructed of carbon-fiber prepreg laminate forming a leading-edge spar and chordwise battens. A flexible membrane material is bonded to the spar and batten.

Received 12 August 2004; presented as Paper 2004-4971 at the 22nd Applied Aerodynamics Conference and Exhibit, Providence, RI, 16–19 August 2004; revision received 10 November 2004; accepted for publication 10 November 2004.

*Graduate Student, Department of Mechanical and Aerospace Engineering. Student Member AIAA.

†Distinguished Professor and Chair, Department of Mechanical and Aerospace Engineering; currently Clarence L. "Kelly" Johnson Collegiate Professor and Chair, Department of Aerospace Engineering, University of Michigan, Ann Arbor, Michigan 48109; weishyy@umich.edu. Fellow AIAA.

‡Associate Professor, Department of Mechanical and Aerospace Engineering. Member AIAA.

The wing shape chosen here strives to maximize the wing area, and hence the lift, for a given dimension. However, the tip vortices associated with the present low-aspect-ratio wing also substantially affect the aerodynamics. It is well established that tip vortex causes downwash that modifies the pressure distribution on the wing surface and increases the induced drag. Our interest here is to better understand the fluid physics associated with the tip vortex and induced drag. By gaining deeper insight in this area, we can explore ways to improve the lift-to-drag ratio and flight efficiency. Various methods to reduce the induced drag by decreasing the tip-vortex effects are described in the literature and confirmed by actual applications to aircraft wing design.[4] In this study, we focus on the implication of placing endplates at the wing tip because this is the simplest way from the manufacturing point of view.

The classic linear lifting-line theory[5] is not applicable here because of moderate Reynolds number, small wing aspect ratio, and short distance between the vortex cores in the wake behind the wing that facilitate a strong interaction of the tip vortices. In this study, we employ the numerical approach to investigate the issues.

The effect of endplates on the MAV rigid-wing aerodynamics was previously investigated by Viieru et al.[3] In that study the endplate was simply added to the existing MAV wing to probe its effect on the tip vortex and overall aerodynamics, while the wing shape was retained (see Fig. 2). It was observed that the endplate increases lift by reducing the downwash and increases the effective angle of attack. However, drag increases along with the curved endplate in part because the endplate behaves as a vertically placed airfoil, and the additional form drag causes the overall lift-to-drag ratio to decrease.

Lian and Shyy[6] in their computational analysis, and Waszak et al.[7] in their experimental study, observed that flexible and rigid wings give comparable performance before stall limits. Because the computational cost for the membrane-wing aerodynamics is significantly higher than for the corresponding rigid wing, we will focus on the rigid wing in the present study. For a detailed review of both membrane and rigid-wing aerodynamics, we refer to Lian et al.[8] Specifically, we study the flow over two rigid-wing configurations at angles of attack of 6 and 15 deg. Because a curved endplate deteriorates the overall aerodynamic performances,[3] in this study we have modified the wing platform with endplates, as will be detailed in the following.

Computational Setup

Flow Solver

To compute the aerodynamic performance of the MAV wing, the steady-state, Navier–Stokes equations for the incompressible flow are solved. A pressure-based algorithm[9,10] is used to solve the three-dimensional Navier–Stokes equations written in curvilinear coordinates. A first-order upwind scheme is employed for convection terms, and second-order central difference schemes are adopted for pressure and viscous terms.

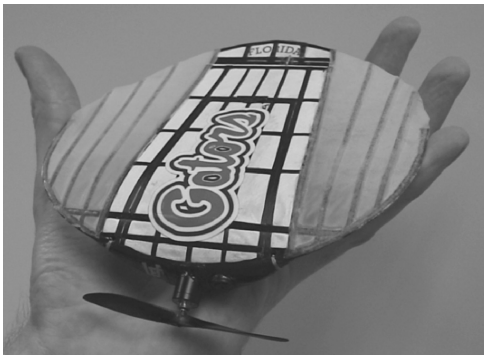

Fig. 1 University of Florida 15-cm micro air vehicle.

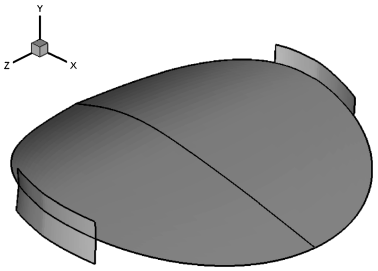

Fig. 2 Initial 15-cm wing and endplates geometry.

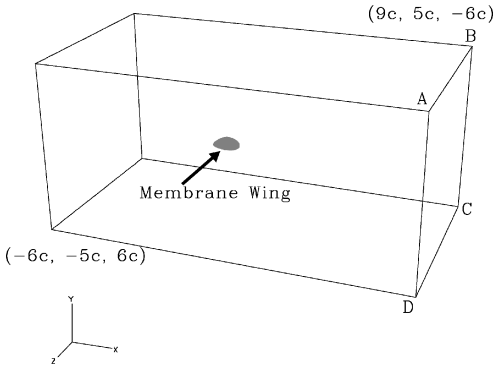

Fig. 3 Computational domain and boundary conditions.

Computational Setup

In this work we focus on the wing while neglecting the fuselage and propeller. The physical problem under consideration is the steady-state flow over a wing in an unbounded domain. The relative position of the wing to the overall computational is shown in Fig. 3, where the open boundary is placed far away from the wing to minimize the effect caused by wave reflection. The structured, multiblock grid is employed in the computation. Because the freestream velocity is along the chordwise direction and no propeller is modeled, only half of the wing is computed based on the symmetry condition. Regarding the inlet and outlet boundary treatments, on surface ABCD, a zero-gradient boundary condition is imposed, whereas all other boundaries are assigned a Dirichlet-type boundary condition.

Three wing geometries have been studied. The original wing (Fig. 4a) has a span of 15 cm, a root chord of 13.3 cm, and a wing area of 160 cm^2. The modified wing (Fig. 4b) has a span of 14 cm and a wing area of 155 cm^2, while the root chord has the same length as the original wing. The endplate attached to the modified wing has a length of 4.4 cm and a height of 3.4 cm. The modified wing with endplates is shown in Fig. 4c.

To confirm the capabilities of the Navier–Stokes solver, the computational results are first compared with wind-tunnel data measured for a MAV rigid wing with 12.5-cm (5-in.) span. The wing tested has a smaller area than the ones used for investigating the endplate; however, the overall shape and aspect ratio are similar.

The experiment was conducted in a horizontal, open-circuit low-speed wind tunnel. It has a square entrance with a bell mouth inlet

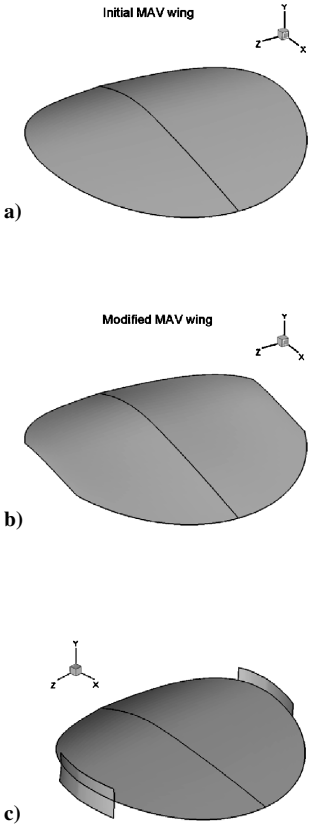

Fig. 4 Wing shape geometry: a) baseline wing, b) modified wing, and c) endplates location on the modified wing.

type and several screens that provide low turbulence levels, less than 0.1%, in the test section. The test section is 91.4 × 91.4 cm and a length of 2 m. The model under test is attached to a six-components internal sting balance. The angle of attack is controlled by computer and can be set in any sequence, steady or variable in time. The force balance was calibrated from 1 to 500 g, from precisely defined loading points. For more detailed information of the experimental measurement and uncertainty, we refer to Albertani et al.[11]

The 12.5-cm wing configuration was tested at two different Reynolds numbers (7.1×10^4 and 9.1×10^4) based on the root-chord length. The experimental data were obtained by averaging the values from multiple tests for each angle of attack and Reynolds number. In Fig. 5a the lift vs drag curves are plotted for the two Reynolds numbers just mentioned. The figure demonstrates good agreement between computational and experimental data. As shown in Fig. 5b, within the range of the Reynolds number considered here, the lift-to-drag ratio does not vary much. Furthermore, both experiment and computation show that the best lift-to-drag ratio is reached for an angle of attack between 6 and 9 deg.

Lian and Shyy[6] have performed computations for the same original wing geometry (Fig. 4a) using three different grid sizes ranging from 180,000 nodes at the coarse level and 2.3 million nodes at the fine level. They conclude that the coarse-grid solution underpredicts the lift-to-drag ratio C_L/C_D by 0.5% and form drag force by less than 0.7% compared to the finest grid solution. A similar result was also obtained for the lift force. However, the skin-friction drag is sensitive to grid nodes density, and the computation based on the coarse mesh overestimates it by 10%. Because in the presently considered parameter range the form drag is at least one order of magnitude higher than the viscous drag, we use the coarse grid in our computations.

Tip Vortex and Endplate Effect

Based on the freestream velocity and the root-chord length, the Reynolds number of 9×10^4 is adopted for the wing configurations in all cases discussed next.

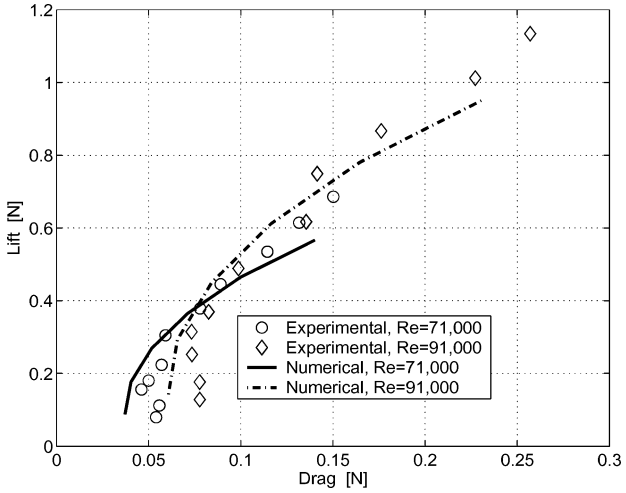

a) Lift-drag polar plot

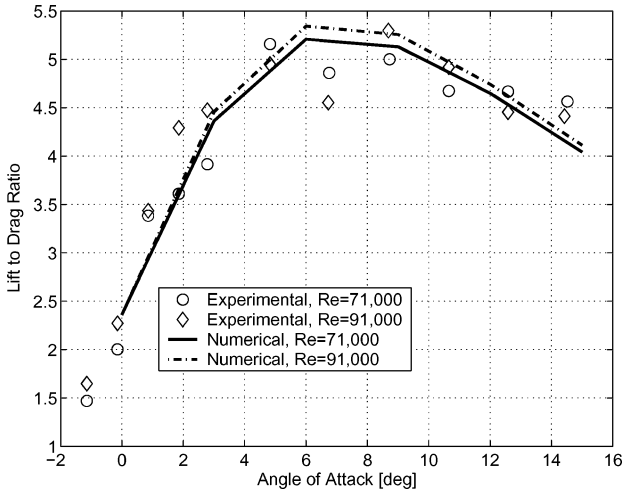

b) Lift-to-drag ratio vs angle of attack

Fig. 5 Numerical and experimental assessment of lift and drag for different Reynolds number and angles of attack.

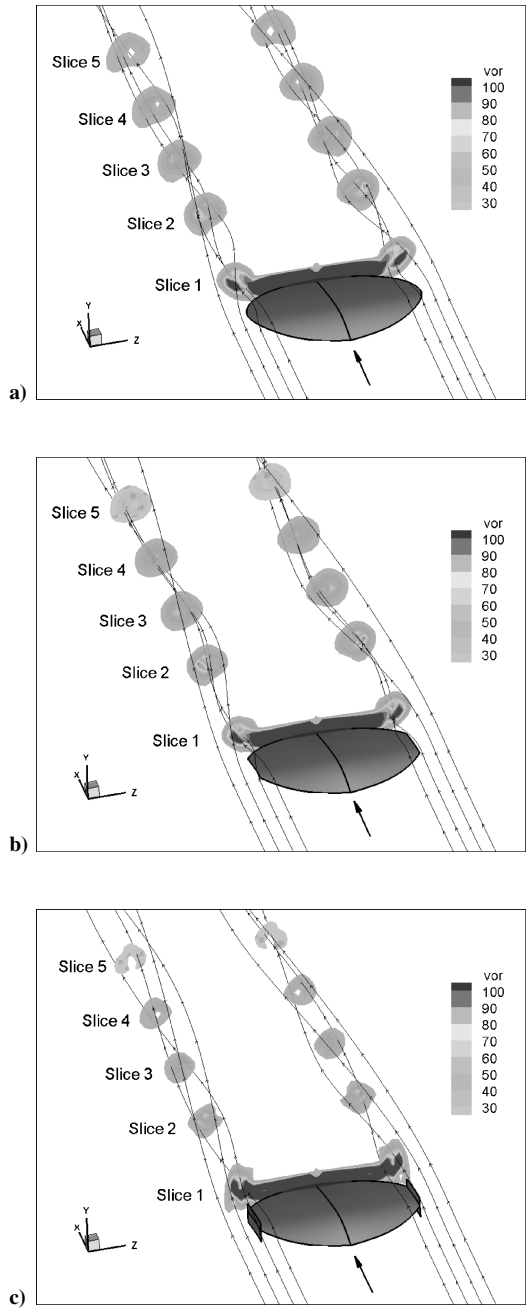

Fig. 6 Vorticity contours behind the wing at 6-deg angle of attack: a) original wing, b) modified wing without endplates, and c) modified wing with endplates.

Wake Behind the Wing

The circulatory motion over the wing tip is induced by the pressure difference between the high-pressure region below the wing surface and the low-pressure region above the wing. The tip vortex can be directly observed from the streamlines. In Fig. 6 the vorticity magnitude contours behind the wing are plotted in planes perpendicular to the x axis, that is, the streamwise direction. From this figure one can see that the strongest wake vortex is located near the wing tip, indicating that the circulation gradient is the largest there. The effect of the endplates can be observed from their influence on the wake behind the wing. Generally both wings without the endplates show stronger tip-vortex effects compared to the wing with the endplates attached. Also from Fig. 6c one can see that endplates directly influence the circulation and vortex structures in the wing-tip region, which is consistent with the observations made by LaRoche and Palffy.[4]

One can observe the vortex intensity and the circulation associated with it by looking at the slices perpendicular to the streamwise direction (x axis) behind the wing. Downstream the flow can be approximated with the flow around a vortex core of constant rotation and a potential motion outside the core. The relation between the pressure at the vortex center and the circulation around a rigid rotating body is given by[12]

$$\Gamma^2 = 4\pi^2 r_1^2 p_{\text{center}}/\rho \tag{1}$$

where r_1 is the rigid-body radius, p_{center} is the pressure at the rigid-body center, and ρ is the fluid density. Equation (1) shows that the vortex strength, measured by its circulation, is proportional with the pressure drop in the vortex core and its radius. In Fig. 7, the pressure coefficient is plotted along the vortex core diameter at $x/c = 3$ behind the wing and $x/c = 5$. The amount of pressure drop inside the vortex core indicates that the endplates reduce the vortex strength. Also the modified wing without the endplates shows the strongest vortex.

Influence of the Endplates on the Flow over the Wing

Tip vortex modifies the local flowfield by creating an induced vertical velocity that decreases the local angle of attack and results in a component of the total force on the wing in the drag direction known as induced drag.

The total drag coefficient for a high-Reynolds-number wing can be written as[13]

$$C_D = C_{D,p} + C_{D,f} + C_L^2 \big/ (\pi \cdot e \cdot \text{AR}) \tag{2}$$

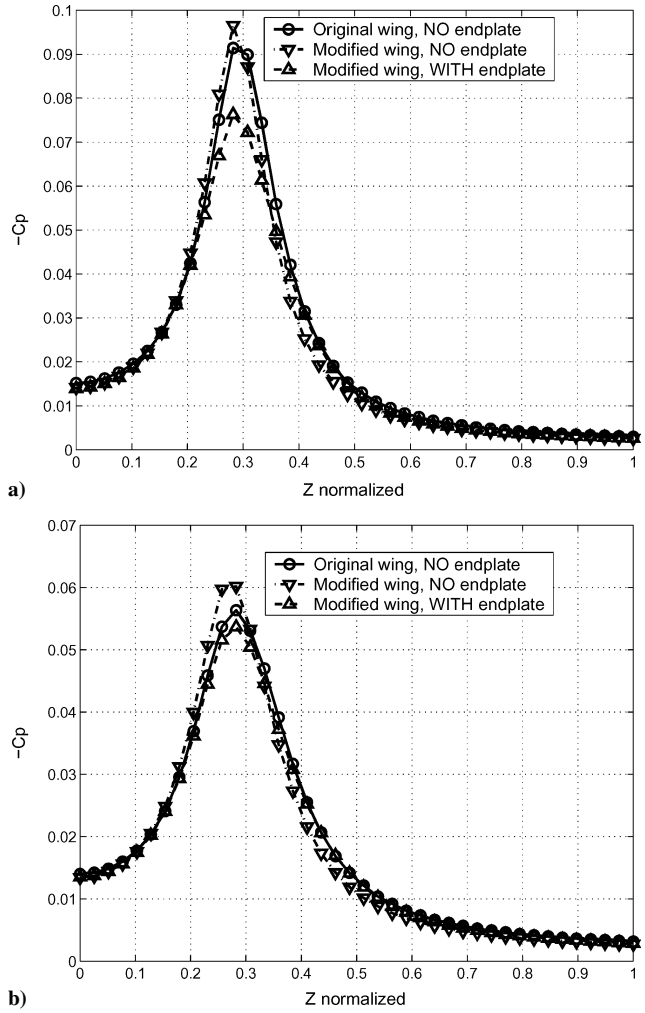

Fig. 7 Pressure coefficient along the vortex core behind the wing at 6-deg angle of attack: a) $x/c = 3$ (slice 3) and b) $x/c = 5$ (slice 5).

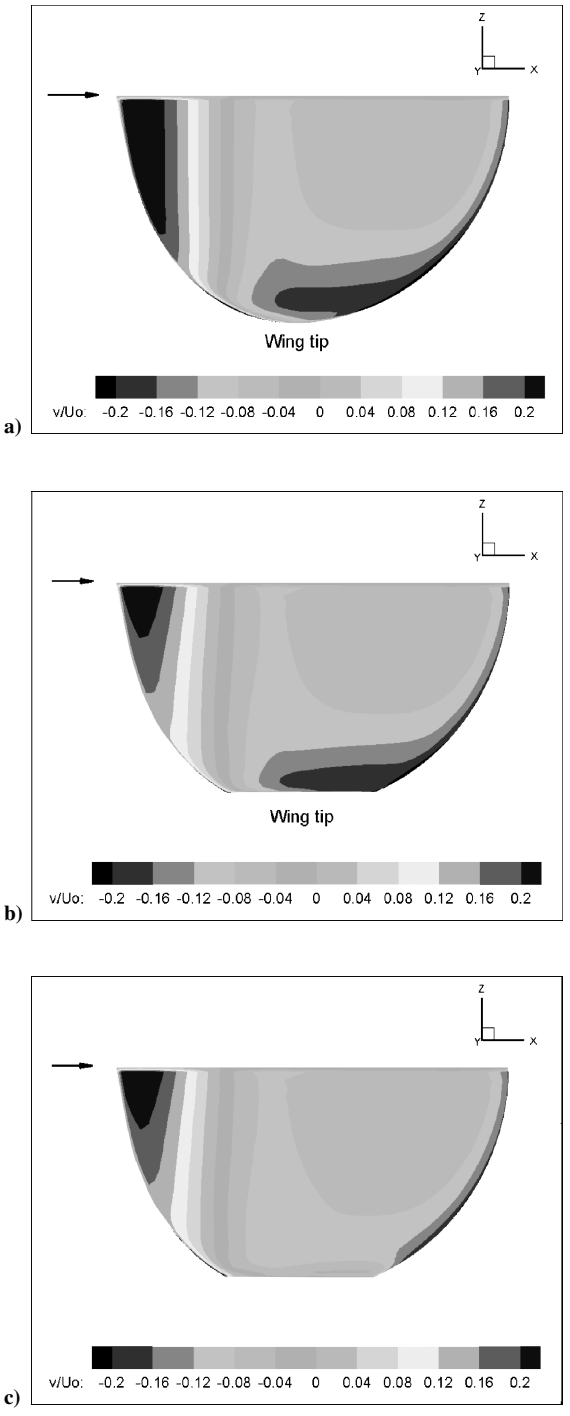

Fig. 8 Vertical velocity contours slightly above the wing at 6-deg angle of attack: a) original wing, b) modified wing without endplates, and c) modified wing with endplates.

where e is the span efficiency factor, which has a range between 0.7 and 1. Therefore, the total drag is composed of three parts: drag component of the total aerodynamic force obtained by integrating the pressure the wing surface $C_{D,p}$, drag caused by friction on the wing surface $C_{D,f}$, and induced drag $C_L^2/(\pi \cdot e \cdot AR)$. Although Eq. (2) is applicable only for high-Reynolds-number wings, it is useful to help interpret the interplay of the wing aspect ratio and induced drag. Overall, the tip vortex has stronger effects on lower-aspect-ratio wings.

The endplate basically deters the flow from the high-pressure region on the lower wing surface to reach the low-pressure region on the upper wing surface. One effect of the endplate attached to both wing shapes is a reduction of the vertical velocity induced by the tip vortex in an area near the wing tip, as one can see by comparing the vertical velocity contours plotted in Fig. 8a for the original wing shape and Figs. 8b and 8c for the modified wing shape.

In Fig. 9 pressure contours on the wing surface and the streamlines on a surface parallel to the wing surface slightly above the wing are plotted. The tip vortex is formed at the leading edge near the tip by the pressure difference between wing sides. The initiation of the tip vortex occurs at almost the same location along the leading edge, as indicated in Figs. 9a and 9b. The low-pressure zone on the upper wing surface near the wing tip associated with the vortex core can be visualized. This low-pressure zone is also observable in the spanwise pressure coefficient plot on the upper wing surface (Figs. 10a and 11a). The low-pressure zone inside the vortex accelerates the fluid near the tip and indicates the area affected by the tip vortex.

In Fig. 12 the pressure contours on the lower wing surface as well as the streamlines on a surface parallel with the wing surface slightly below the wing are plotted. The pressure difference between the high-pressure zone (in the lower wing surface area) and the low-pressure zone (in the upper wing surface area) induces a spanwise flow that bends the streamlines toward the wing tip and accelerates the flow near the tip as one can see in Figs. 12a and 12b. The pressure drop near the wing tip in the absence of the endplate can also be recognized in the spanwise pressure coefficient plot on the lower wing surface (also see Figs. 10b and 11b).

Endplate Effect on Pressure Distribution on the Wing Surface

From the pressure contours and horizontal velocity contours, we notice that the endplate affects the flowfield over the wing. The endplate slows down the flow near the wing tip. This decrease in velocity reduces the pressure drop on the upper wing surface corresponding to the vortex core (Figs. 10a and 11a). On the other hand, a lower

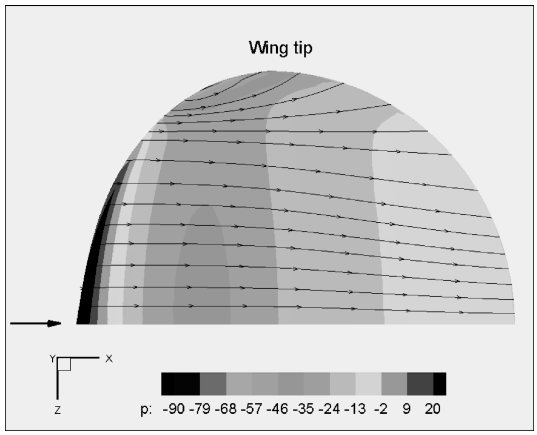

a)

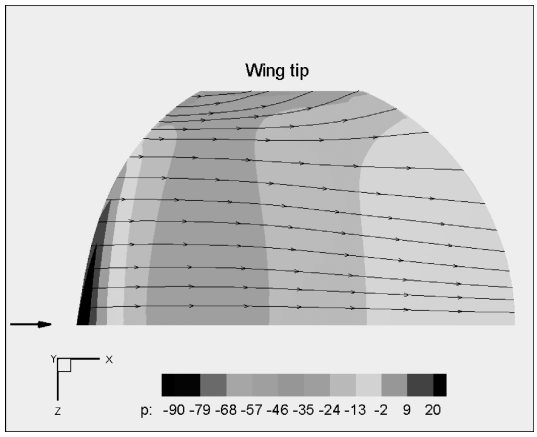

b)

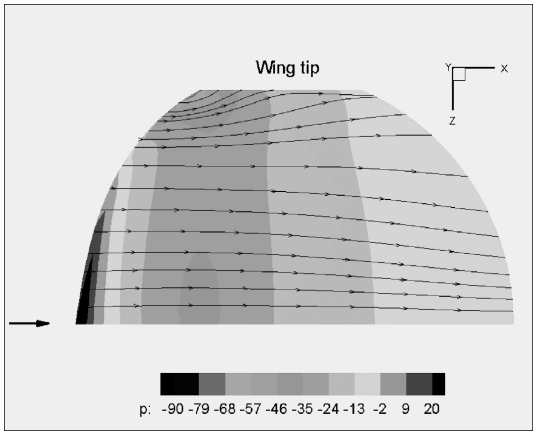

c)

Fig. 9 Pressure contours on the wing upper surface and streamlines slightly above the wing at 6-deg angle of attack: a) original wing, b) modified wing without endplates, and c) modified wing with endplates. (Pressure units are N/m^2.)

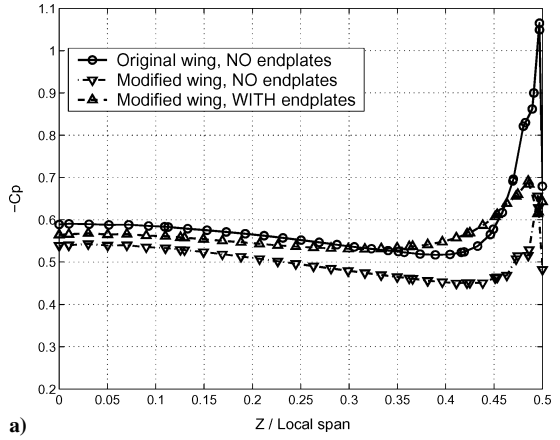

a)

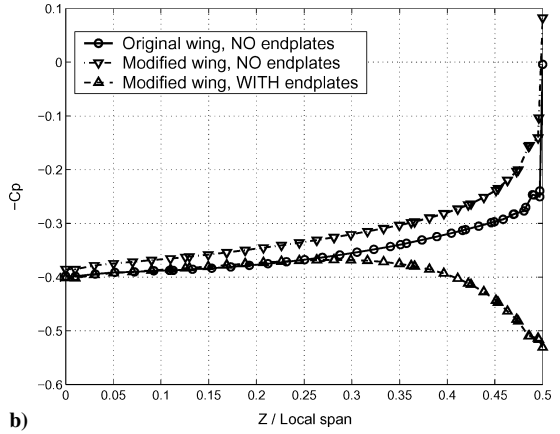

b)

Fig. 10 Pressure coefficient on the wing surface at $x/c = 0.34$ and 6-deg angle of attack: a) wing upper surface and b) wing lower surface.

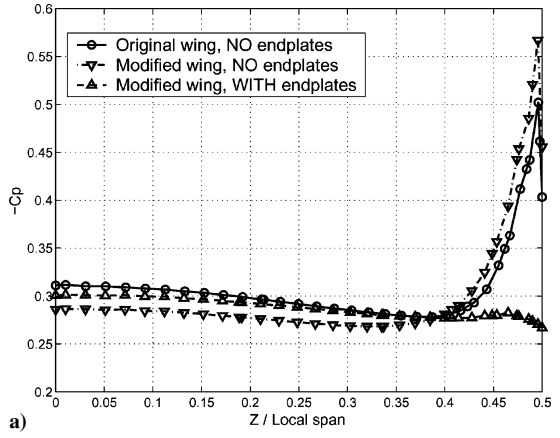

a)

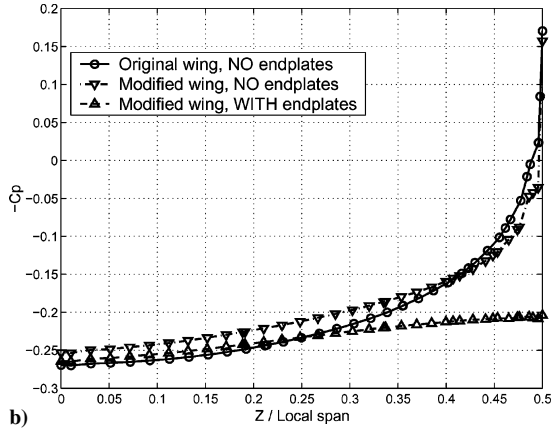

b)

Fig. 11 Pressure coefficient on the wing surface at $x/c = 0.53$ and 6-deg angle of attack: a) wing upper surface and b) wing lower surface.

velocity slightly below the wing increases the high-pressure area there because more momentum is transferred to the wing as pressure instead of being shed as vorticity at the wing tip. The increase in high-pressure zone on the lower wing surface in the presence of the endplate can be clearly seen from the spanwise pressure coefficient on the lower wing surface plot (Figs. 10b and 11b) and also from the pressure contours on the lower wing surface shown in Fig. 12.

In Fig. 13 the spanwise lift distribution obtained by integrating the pressure difference along the local chord at specified spanwise location is plotted. We notice that when the endplates are attached the lift is increased compared with the wing shape without the endplate.

The modified wing with the endplates produces almost the same amount of lift as the original wing. However, if we look at the

Table 1 Aerodynamic forces at 6-deg angle of attack

AoA = 6 deg	Original MAV wing No endplates	Modified MAV wing No endplates	Modified MAV wing with endplates
Lift, N	0.49	0.44	0.49
Drag, N	0.074	0.065	0.067
Lift/drag	6.64	6.85	7.39

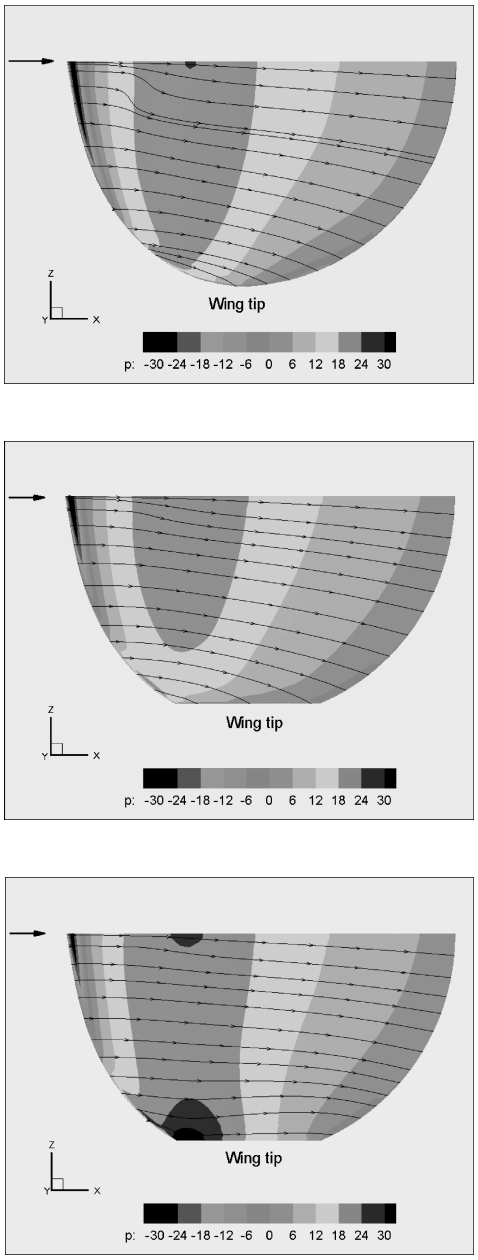

Fig. 12 Pressure contours on the wing lower surface and streamlines slightly below the wing at 6-deg angle of attack: a) original wing, b) modified wing without endplates, and c) modified wing with endplates. (Pressure units are N/m^2.)

spanwise drag distribution plotted in Fig. 14 the modified wing with or without endplate offers the lowest drag for the almost 75% of the half wing span starting from the root.

In Table 1 the overall aerodynamic performances parameters are presented for 6-deg angle of attack (AoA). Lift and drag are computed by integrating the pressure difference over the entire wing surface and the endplate surface. In Table 2 the same parameters are presented for an angle of attack of 15 deg.

From the tables, for an angle of attack of 6 deg, we see an improvement in lift-to-drag ratio of 10.1% for the modified wing configuration with endplates compared with the baseline configuration (original wing, no endplate). This improvement is based mainly on the reduction in drag offered by the modified wing shape because the lift forces are closed.

Table 2 Aerodynamic forces at 15-deg angle of attack

AoA = 15 deg	Original MAV wing No endplates	Modified MAV wing No endplates	Modified MAV wing with endplates
Lift, N	0.92	0.86	0.87
Drag, N	0.22	0.21	0.21
Lift/drag	4.16	4.15	4.22

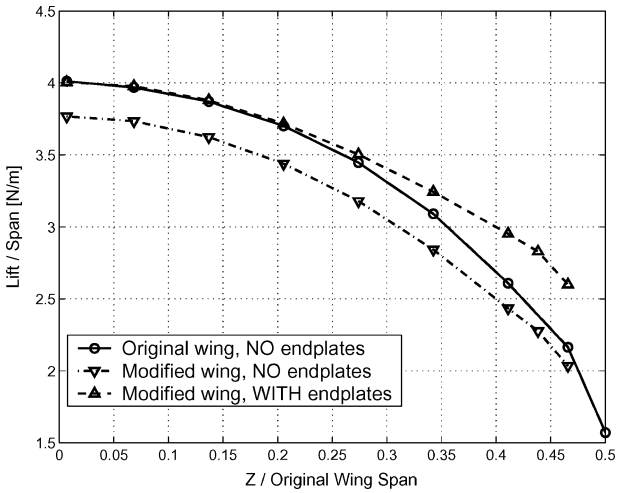

Fig. 13 Spanwise lift distribution at 6-deg angle of attack.

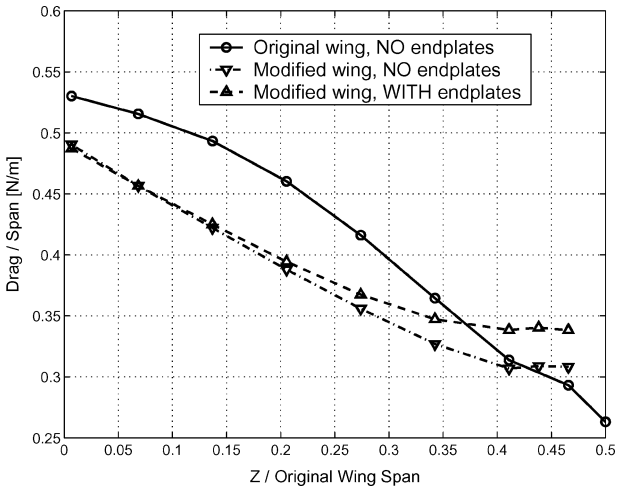

Fig. 14 Spanwise drag distribution at 6-deg angle of attack.

For 15-deg angle of attack the modified wing with endplates shows an increase of 1.4% in lift-to-drag ratio compared with the baseline configuration. This is achieved by an important reduction of drag. Lift is decreasing in this case with almost 5%.

Summary

A numerical study is performed to analyze the aerodynamic performance of a micro-air-vehicle (MAV) rigid wing. The influence of the wing-tip shape on the tip vortex and the aerodynamic performances was studied. Also the endplate shape influence over the overall wing aerodynamic was studied as a method to enhance the lift-to-drag ratio as a measure of flight efficiency. We solved the full incompressible Navier–Stokes equations for 6- and 15-deg angles of attack, for both wing shapes with and without the endplate.

We observed the following:

1) The modified wing shape reduces the drag either with endplate or without. However the lift is also reduced because of stronger vortex and reduced area.

2) The endplate parallel to the freestream velocity increases lift without a significant increase in drag. The increase in lift is more near the tip where the endplate reduces the flow from going from the lower surface to the upper surface of the wing, reducing the downwash, and increasing the effective angle of attack and consequently the lift increases.

3) The effectiveness of the endplate diminishes as the angle of attack increases because of stronger wing tip vortex.

Further investigations related to the high-angles-of-attack flows will help our understanding and treatment of the tip-vortex effects on low-aspect MAV wings.

Acknowledgment

The present work has been supported by the U.S. Air Force.

References

[1]Shyy, W., Berg, M., and Ljungqvist, D., "Flapping and Flexible Wings for Biological and Micro Vehicles," *Progress in Aerospace Sciences*, Vol. 35, July 1999, pp. 455–506.

[2]Ifju, G. P., Jenkins, D., Ettinger, S., Lian, Y., Shyy, W., and Waszak, R. M., "Flexible-Wing-Based Micro Air Vehicles," AIAA Paper 2002-0705, Jan. 2002.

[3]Viieru, D., Lian, Y., Shyy, W., and Ifju, G. P., "Investigation of Tip Vortex on Aerodynamic Performance of a Micro Aerial Vehicle," AIAA Paper 2003-3597, June 2003.

[4]LaRoche, U., and Palffy, S., "Wing Grid, a Novel Device for Reduction of Induced Drag on Wings," International Council of the Aeronautical Sciences, Sept. 1996.

[5]Katz, J., and Plotkin, A., *Low-Speed Aerodynamics*, 2nd ed., Cambridge Univ. Press, Cambridge, MA, 2002, pp. 167–183.

[6]Lian, Y., and Shyy, W., "Three-Dimensional Fluid-Structure Interactions of a Membrane Wing for Micro Air Vehicle Applications," AIAA Paper 2003-1726, April 2003.

[7]Waszak, R. M., Jenkins, N. L., and Ifju, G. P., "Stability and Control Properties of an Aeroelastic Fixed Wing Micro Aerial Vehicle," AIAA Paper 2001-4005, Aug. 2001.

[8]Lian, Y., Shyy, W., Viieru, D., and Zhang, B., "Membrane Wing Aerodynamics for Micro Air Vehicles," *Progress in Aerospace Sciences*, Vol. 39, Aug.–Oct. 2003, pp. 425–465.

[9]Thakur, S., Wright, J., and Shyy, W., "STREAM: A Computational Fluid Dynamics and Heat Transfer Navier–Stokes Solver. Theory and Applications," Streamline Numerics, Inc., and Computational Thermo-Fluid Lab., Dept. of Mechanical and Aerospace Engineering, Technical Rept., Gainesville, FL, Sept. 2002.

[10]Shyy, W., *Computational Modeling for Fluid Flow and Interfacial Transport*, Elsevier, Amsterdam, The Netherlands, 1997, pp. 113–238.

[11]Albertani, R., Hubner, P., Ifju, P. G., Lind, R., and Jackowski, J., "Wind Tunnel Testing of Micro Air Vehicles at Low Reynolds Numbers," Society of Automotive Engineers, Paper 2004-01-3090, Nov. 2004.

[12]Prandtl, L., and Tietjens, O. G., *Fundamentals of Hydro And Aeromechanics*, Dover, New York, 1957, pp. 212–215.

[13]Anderson, J. D., Jr., *Introduction to Flight*, 3rd ed., McGraw–Hill, New York, 1989, pp. 216–226.